3

Effective Moduli of a Continuous Fiber-Reinforced Lamina

3.1 Introduction

In the previous chapter, the concept of an effective modulus was found to be essential to the development of practical engineering stress–strain relationships for composite materials. Recall that for some representative volume element (RVE) in a heterogeneous composite, the volume-averaged stresses can be related to the volume-averaged strains by the effective moduli of an equivalent homogeneous material. Chapter 2 was primarily concerned with the development and manipulation of macromechanical stress–strain relationships involving the lamina effective moduli, however, and the roles of lamina constituent materials were not examined in detail. In this chapter, we will discuss various micromechanical models for predicting the effective moduli of continuous fiber-reinforced laminae in terms of the corresponding material properties, relative volume contents, and geometric arrangements of the fiber and matrix materials. Corresponding models for predicting strength and hygrothermal properties will be presented in chapter 4 and chapter 5, respectively. Micromechanics of discontinuous fiber composites, including nanocomposites, is covered in chapter 6.

Before proceeding further, it is appropriate to discuss briefly the term "micromechanics." To a materials scientist, the term may imply the study of mechanical behavior at the level of molecular or crystal structures. Since the behavior of composite material structures such as laminates is referred to as "macromechanics," it has been suggested that, perhaps, mechanics of composites at the constituent material level should be referred to as "minimechanics" [1]. In the present context, and in much of the composites literature, however, the analysis of effective composite properties in terms of constituent material properties is called "micromechanics." The terms "structure–property relationships" and "effective modulus theories" are also used in the literature. Many analytical approaches have been developed over the years, and comprehensive literature surveys have

been published by Chamis and Sendeckyj [2], Christensen [3], Hashin [1], and Halpin [4].

Micromechanical analyses are based on either the mechanics of materials or the elasticity theory. In the mechanics of materials approach, simplifying assumptions make it unnecessary to specify the details of the stress and strain distributions at the micromechanical level, and fiber-packing geometry is generally arbitrary. The theory of elasticity models involves the solution for actual stresses and strains at the micromechanical level, and fiber-packing geometry is taken into account. The elasticity approach often involves numerical solutions of the governing equations because of the complex geometries and boundary conditions. Although the simplifying assumptions used in the mechanics of materials approach violate some of the laws of elasticity theory, some of the results are sufficiently accurate that they are often used in design. A third category involves empirical solutions that are based on curve-fitting to elasticity solutions or experimental data, and some of these equations are often used along with the mechanics of materials equations to formulate a complete set of simple lamina design equations.

Ideally, micromechanical models should enable us to answer quickly "What if?" questions regarding the effects of various fiber/matrix combinations without actually fabricating and testing the composites in question. On the other hand, experience has shown that there are pitfalls in such an approach and that there is no substitute for experimental characterization. Experimental data on the constituent material properties are required as input to the models, and similar data on the corresponding composite properties are required in order to assess the validity of the models. Indeed, as we will see later, some properties such as fiber transverse moduli are usually inferred from the micromechanical model and other measured properties because of the difficulty of direct measurement. Once a micromechanical model has been shown to be sufficiently accurate by comparison with experiment, however, it can become part of a powerful design methodology that enables us to design the material as well as the structure. Aside from design implications, micromechanical analysis and experimental characterization are both essential if we are to understand better "how composites work."

One of the key elements in micromechanical analysis is the characterization of the relative volume or weight contents of the various constituent materials. We will find that the micromechanics equations involve constituent volume fractions, but actual measurements are often based on weight fractions. Measurements are discussed later, but the relationships between volume fractions and weight fractions will be presented here.

For any number of constituent materials, n, the sum of the constituent volume fractions must be unity:

$$\sum_{i=1}^{n} \upsilon_i = 1 \tag{3.1}$$

where $\upsilon_i = V_i/V_c$ = volume fraction of the ith constituent, V_i = volume of the ith constituent, V_c = total volume of the composite.

In many cases this equation reduces to

$$\upsilon_f + \upsilon_m + \upsilon_v = 1 \tag{3.2}$$

where υ_f, υ_m, and υ_u are the volume fractions of the fiber, matrix, and voids, respectively. The corresponding equations for weight fractions are

$$\sum_{i=1}^{n} w_i = 1 \tag{3.3}$$

and

$$w_f + w_m = 1 \tag{3.4}$$

where $w_i = W_i/W_c$, $w_f = W_f/W_c$, $w_m = W_m/W_c$, and W_i, W_f, W_m, and W_c are the weights of the ith constituent, fibers, matrix, and composite, respectively. Note that the weight of the voids has been neglected here. Substituting the product of density and volume for weight in each term of equation (3.3) and equation (3.4) and solving for the composite density, we get the "rule of mixtures":

$$\rho_c = \sum_{i=1}^{n} \rho_i \upsilon_i \tag{3.5}$$

or

$$\rho_c = \rho_f \upsilon_f + \rho_m \upsilon_m \tag{3.6}$$

where ρ_i, ρ_f, ρ_m, and ρ_c are the densities of the ith constituent, fiber, matrix, and composite, respectively. Similarly, equation (3.1) and equation (3.2) can be rearranged as

$$\rho_c = \frac{1}{\sum_{i=1}^{n} (w_i/\rho_i)} \tag{3.7}$$

and

$$\rho_c = \frac{1}{(w_f/\rho_f)+(w_m/\rho_m)} \tag{3.8}$$

Equation (3.2) can also be rearranged so that the void fraction can be calculated from measured weights and densities:

$$v_v = 1 - \frac{(W_f/\rho_f)+(W_c - W_f)/\rho_m}{W_c/\rho_c} \tag{3.9}$$

Typical autoclave-cured composites may have void fractions in the range 0.1 to 1%. Without vacuum bagging, however, volatiles trapped in the composite during the cure cycle can cause void contents of the order of 5%.

In order to get some idea as to the range of constituent volume fractions that may be expected in fiber composites, it is useful to consider representative area elements for idealized fiber-packing geometries such as the square and triangular arrays shown in figure 3.1. If we assume that the fiber spacing, s, and the fiber diameter, d, do not change along the fiber length, then the area fractions must be equal to the volume fractions. Indeed, optical determination of area fractions is possible from

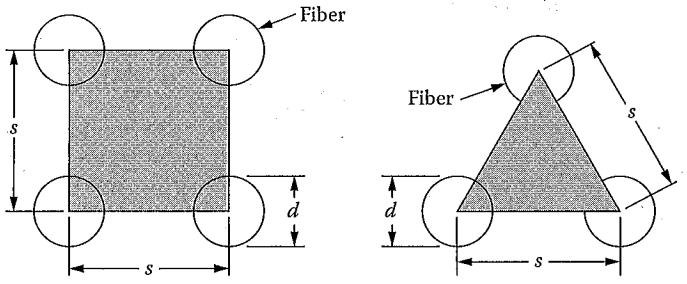

FIGURE 3.1
Representative area elements for idealized square and triangular fiber-packing geometries.

micrographs. The fiber volume fraction for the square array is found by dividing the area of fiber enclosed in the shaded square by the total area of the shaded square [5]:

$$v_f = \frac{\pi}{4}\left(\frac{d}{s}\right)^2 \tag{3.10}$$

Clearly, the maximum theoretical fiber volume fraction occurs when $s = d$. In this case,

$$v_{f\,max} = \frac{\pi}{4} = 0.785$$

A similar calculation for the triangular array shows that

$$v_f = \frac{\pi}{2\sqrt{3}}\left(\frac{d}{s}\right)^2 \tag{3.12}$$

and when $s = d$, the maximum fiber volume fraction is

$$v_{f\,max} = \frac{\pi}{2\sqrt{3}} = 0.907 \tag{3.13}$$

The close packing of fibers required to produce these theoretical limits is generally not achievable in practice, however. In most continuous fiber composites, the fibers are packed in a random fashion as shown in figure 3.2, and the fiber volume fractions range from 0.5 to 0.8. In short fiber composites, fiber volume fractions are usually much lower due to processing limitations (e.g., the viscosity of the fiber/resin mixture must be controlled for proper flow during molding) and the random orientation of fibers. Since fiber-packing geometry is never entirely repeatable from one piece of material to another, we should not expect our micromechanics predictions to be exact.

The random nature of the fiber-packing geometry in real composites such as the one shown in figure 3.2 can be quantified by the use of the Voronoi cell (fig. 3.3) and a statistical distribution describing the Voronoi cell size [6]. Each point within the space of a Voronoi cell for a particular fiber is closer to the center of that fiber than it is to the center of any other fiber. If we can approximate the Voronoi cell in figure 3.3(a) as an equivalent square area as shown in figure 3.3(b) and figure 3.3(c), then equation (3.10) can be used to describe the relationship between the fiber diameter d, the fiber

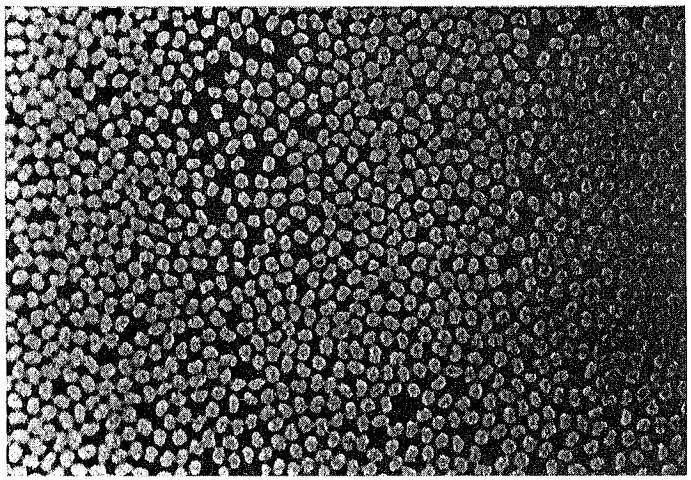

FIGURE 3.2
Photomicrograph of carbon/epoxy composite showing actual fiber-packing geometry at 400 × magnification.

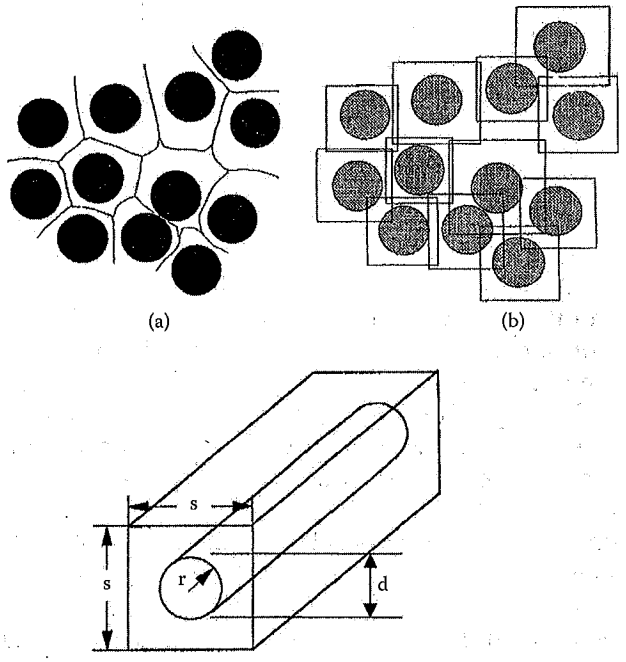

FIGURE 3.3
Voronoi cell and its approximation. (From Yang, H. and Colton, J.S. 1994. *Polymer Composites*, 51, 34–41. With permission.)

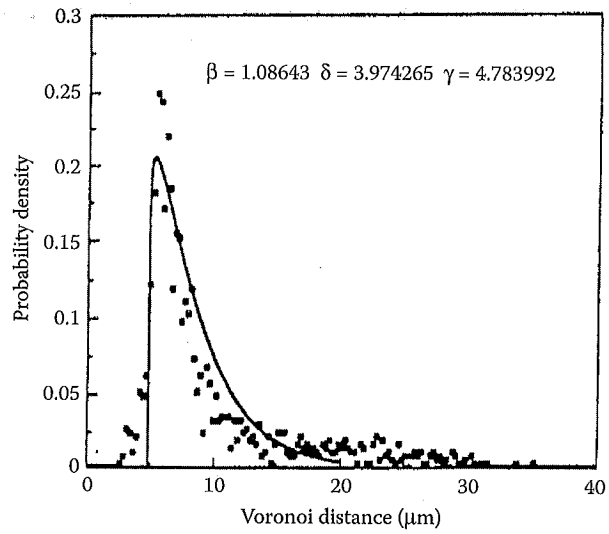

FIGURE 3.4
Typical histogram of Voronoi distances and corresponding Wiebull distribution for a thermoplastic matrix composite. (From Yang, H. and Colton, J.S. 1994. *Polymer Composites*, 51, 34–41. With permission.)

volume fraction v_f, and the Voronoi cell size s. Yang and Colton [6] have used digital image processing to show that the Wiebull distribution

$$f(s) = \frac{\beta}{\delta}\left(\frac{s-\gamma}{\delta}\right)^{\beta-1} \exp\left[-\left(\frac{s-\gamma}{\delta}\right)^{\beta}\right] \quad \text{when } s \geq \gamma \tag{3.14}$$

$$f(s) = 0 \quad \text{otherwise}$$

adequately characterizes the probability density function for the Voronoi cell size for several composites, where β, δ, and γ are the Wiebull parameters associated with the shape, scale, and location of the distribution, respectively. A typical histogram of measured Voronoi distances for a thermoplastic matrix composite and the corresponding Wiebull distribution from regression analysis are shown in figure 3.4.

EXAMPLE 3.1

A carbon/epoxy composite specimen has dimensions of 2.54 cm × 2.54 cm × 0.3 cm and a weight of 2.98 g. After "resin digestion" in an acid solution, the remaining carbon fibers weigh 1.863 g. From independent tests, the densities of the carbon

fibers and epoxy matrix materials are found to be 1.9 and 1.2 g/cm³, respectively. Determine the volume fractions of fibers, epoxy matrix, and voids in the specimen.

Solution. The composite density is

$$\rho_c = \frac{2.98\,g}{(2.54)(2.54)(0.3)cm^3} = 1.54\,g/cm^3$$

From equation (3.9), the void fraction is

$$\upsilon_v = 1 - \frac{(1.863/1.9)+(2.98-1.863)/1.2}{2.98/1.54} = 0.0122 \quad \text{or} \quad 1.22\%$$

From equation (3.2),

$$v_f + \upsilon_m = 1 - \upsilon_v = 1.0 - 0.0122 = 0.988$$

Then, from equation (3.6),

$$1.54 = 1.9v_f + 1.2(0.988 - v_f)$$

Therefore, the fiber volume fraction is

$$\upsilon_f = 0.506 \text{ or } 50.6\%$$

and the matrix volume fraction is

$$\upsilon_m = 0.988 - 0.506 = 0.482 \text{ or } 48.2\%$$

EXAMPLE 3.2

Assume that the carbon fibers in the specimen from example 3.1 have been uniformly coated with an epoxy "sizing" of thickness t before bonding of the fibers and matrix together to form a unidirectional composite. If the bare fibers have a diameter d = 0.0005 in (0.0127 mm) and the coated fibers are assumed to be packed together in the tightest possible square array, what is the thickness of the sizing?

Solution. The fiber spacing, s, which must be equal to the coated fiber diameter, d_c, can be found from equation (3.10):

$$s = d_c = \sqrt{\frac{\pi d^2}{4\upsilon_f}} = \sqrt{\frac{\pi(0.0005)^2}{4(0.506)}} = 0.000623 \text{ in } (0.0158 \text{ mm})$$

The thickness is then $t = (d_c - d)/2 = 0.0000615$ in (0.00156 mm).

3.2 Elementary Mechanics of Materials Models

The objective of this section is to present elementary mechanics of materials models for predicting four independent effective moduli of an orthotropic continuous fiber-reinforced lamina. In the elementary mechanics of materials approach to micromechanical modeling, fiber-packing geometry is not specified, so that the RVE may be a generic composite block consisting of fiber material bonded to matrix material, as shown in figure 3.5. More sophisticated mechanics of materials models, which do consider fiber-packing geometry, will be discussed later.

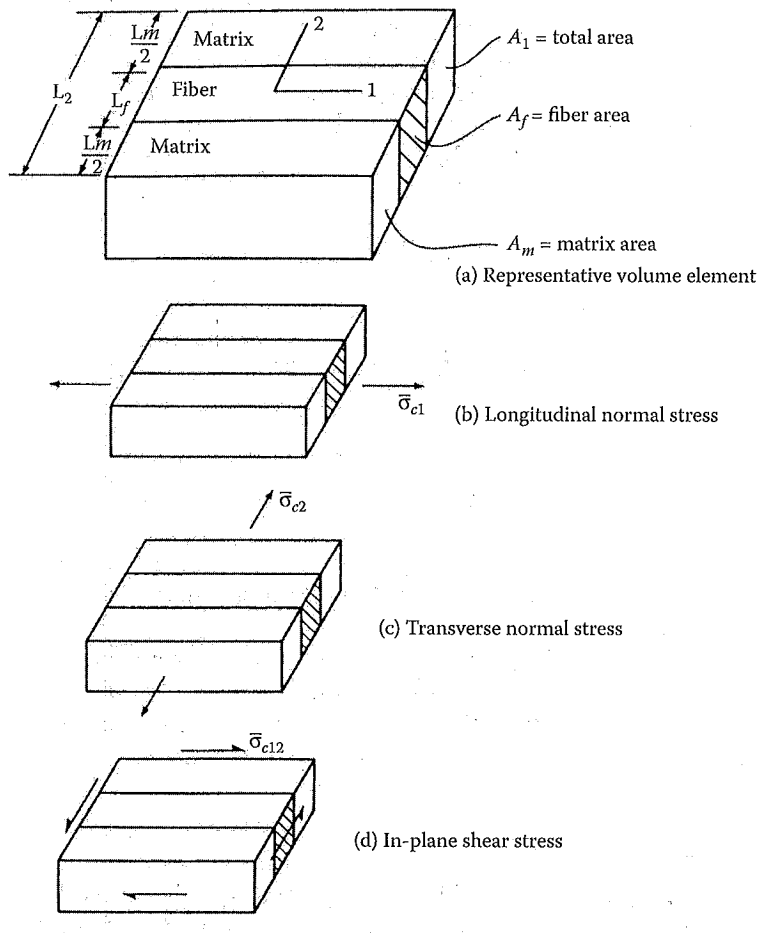

FIGURE 3.5
RVE and simple stress states used in elementary mechanics of materials models.

The constituent volume fractions in the RVE are assumed to be the same as those in the actual composite. Since it is assumed that the fibers remain parallel and that the dimensions do not change along the length of the element, the area fractions must equal the volume fractions. Perfect bonding at the interface is assumed, so that no slip occurs between fiber and matrix materials. The fiber and matrix materials are assumed to be linearly elastic and homogeneous. The matrix is assumed to be isotropic, but the fiber can be either isotropic or orthotropic. Following the concept of the RVE, the lamina is assumed to be macroscopically homogeneous, linearly elastic, and orthotropic.

Micromechanics equations will be developed from either equilibrium or compatibility relationships and assumptions about either stresses or strains in the RVE that has been subjected to a simple state of stress. Since the mechanics of materials approach does not require the specification of the stresses, strains, and displacements at each point, we only deal with the corresponding volume-averaged quantities. Finally, since it is assumed that the stresses, strains, displacements, and RVE dimensions do not change along the length, we can just use area averages:

$$\bar{\sigma} = \frac{1}{V}\int \sigma \, dV = \frac{1}{A}\int \sigma \, dA \tag{3.15}$$

$$\bar{\varepsilon} = \frac{1}{V}\int \varepsilon \, dV = \frac{1}{A}\int \varepsilon \, dA \tag{3.16}$$

$$\bar{\delta} = \frac{1}{V}\int \delta \, dV = \frac{1}{A}\int \delta \, dA \tag{3.17}$$

where the overbar denotes an averaged quantity, and σ = stress, ε = strain, δ = displacement, V = volume, and A = area associated with the face on which loading is applied.

The volume averaging (or area averaging) may occur over the composite lamina, the fiber, or the matrix, and the corresponding parameters will be identified by using subscripts as defined in the following derivations.

3.2.1 Longitudinal Modulus

If the RVE in figure 3.5(a) is subjected to a longitudinal normal stress, $\bar{\sigma}_{c1}$, as shown in figure 3.5(b), the response is governed by the effective longitudinal modulus, E_1. Static equilibrium requires that the total resultant force on the element must equal the sum of the forces acting on the fiber

and matrix. Combining the static equilibrium condition with equation (3.15), we get

$$\bar{\sigma}_{c1}A_1 = \bar{\sigma}_{f1}A_f + \bar{\sigma}_{m1}A_m \tag{3.18}$$

where subscripts c, f, and m refer to composite, fiber, and matrix, respectively, and the second subscript refers to the direction. Since area fractions are equal to the corresponding volume fractions, equation (3.18) can be rearranged to give a "rule of mixtures" for longitudinal stress:

$$\bar{\sigma}_{c1} = \bar{\sigma}_{f1}\upsilon_f + \bar{\sigma}_{m1}\upsilon_m \tag{3.19}$$

Under the assumptions that the matrix is isotropic, that the fiber is orthotropic, and that all materials follow a 1-D Hooke's law (i.e., Poisson strains are neglected),

$$\bar{\sigma}_{c1} = E_1\bar{\varepsilon}_{c1}; \qquad \bar{\sigma}_{f1} = E_{f1}\bar{\varepsilon}_{f1}; \qquad \bar{\sigma}_{m1} = E_m\bar{\varepsilon}_{m1} \tag{3.20}$$

and equation (3.19) becomes

$$E_1\bar{\varepsilon}_{c1} = E_{f1}\bar{\varepsilon}_{f1}\upsilon_f + E_m\bar{\varepsilon}_{m1}\upsilon_m \tag{3.21}$$

Double subscripts are used for the fiber modulus since the fiber is assumed to be orthotropic. That is, the longitudinal fiber modulus, E_{f1}, is not necessarily equal to the transverse fiber modulus, E_{f2}. For example, carbon and aramid fibers exhibit orthotropic behavior, whereas glass and boron are practically isotropic. For the isotropic case, it is a simple matter to let $E_{f1} = E_{f2}$. Since the matrix is assumed to be isotropic, the matrix modulus, E_m, does not need a second subscript.

Finally, the key assumption is that, due to perfect bonding the average strains in the composite, fiber, and matrix along the 1 direction are equal:

$$\bar{\varepsilon}_{c1} = \bar{\varepsilon}_{f1} = \bar{\varepsilon}_{m1} \tag{3.22}$$

Substitution of equation (3.22) in equation (3.21) then yields the rule of mixtures for the longitudinal modulus:

$$E_1 = E_{f1}\upsilon_f + E_m\upsilon_m \tag{3.23}$$

This equation predicts a linear variation of the longitudinal modulus with fiber volume fraction, as shown in figure 3.6. Although simple in form, equation (3.23) agrees well with experimental data from ref. [7] (fig. 3.6[b]) and is a useful design equation. The validity of the key assumptions leading to this equation will now be examined by using a strain energy approach.

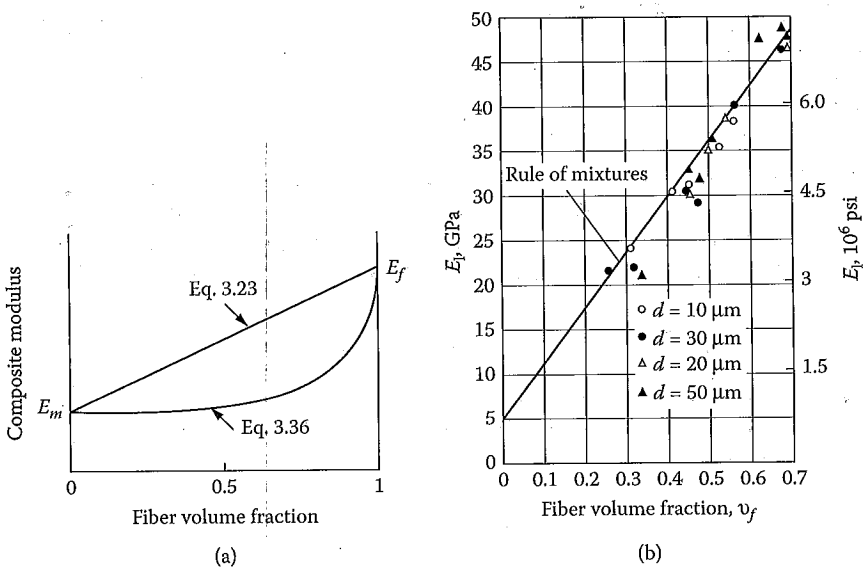

FIGURE 3.6
Variation of composite moduli with fiber volume fraction (a) Predicted E_1 and E_2 from elementary mechanics of materials models, (b) Comparison of predicted and measured E_1 for E-glass/polyester. (From Adams, R.D., 1987. Engineered Materials Handbook, Vol. 1, Composites, 206–217.)

Further insight into the micromechanics of the longitudinal loading case is possible by using a strain energy approach. Under the given state of stress, the total strain energy stored in the composite, U_c, can be represented as the sum of the strain energy in the fibers, U_f, and the strain energy in the matrix, U_m:

$$U_c = U_f + U_m \tag{3.24}$$

Again making the mechanics of materials assumption that the stresses and strains are uniform over the RVE and using equations (3.20), the strain energy terms can be simplified as

$$U_c = \frac{1}{2}\int_{V_c} \sigma_{c1}\varepsilon_{c1}dV = \frac{1}{2}E_1\bar{\varepsilon}_{c1}^2 V_c \tag{3.25a}$$

$$U_f = \frac{1}{2}\int_{V_f} \sigma_{f1}\varepsilon_{f1}dV = \frac{1}{2}E_{f1}\bar{\varepsilon}_{f1}^2 V_f \tag{3.25b}$$

$$U_m = \frac{1}{2}\int_{V_m} \sigma_{m1}\varepsilon_{m1}dV = \frac{1}{2}E_{m1}\bar{\varepsilon}_{m1}^2 V_m \tag{3.25c}$$

In this approximation, the strain energy due to the mismatch in Poisson strains at the fiber/matrix interface has been neglected (recall the assumptions leading to equations [3.20]). This neglected term has been shown to be of the order of the square of the difference between the Poisson's ratios of the fiber and the matrix, so the approximation is justified [8]. It is easily shown that substitution of equation (3.25) in equation (3.24), along with the assumption of equal strains from equation (3.22), again leads to the rule of mixtures given by equation (3.23). But the strain energy approach also allows us to ask, "What happens if the assumption of equal strains is not made?" In order to proceed, let the stresses in the fibers and the matrix be defined in terms of the composite stress as follows:

$$\bar{\sigma}_{f1} = a_1\bar{\sigma}_{c1}; \quad \bar{\sigma}_{m1} = b_1\bar{\sigma}_{c1} \tag{3.26}$$

where a_1 and b_1 are constants. Substitution of equation (3.26) in the rule of mixtures for stress, equation (3.19), leads to

$$a_1 v_f + b_1 v_m = 1 \tag{3.27}$$

Substitution of equation (3.26), equation (3.20), and equation (3.25) in equation (3.24) leads to

$$\frac{1}{E_1} = a_1^2\frac{v_f}{E_{f1}} + b_1^2\frac{v_m}{E_m} \tag{3.28}$$

Note that we did not assume equal strains in fibers and matrix in order to derive these equations. To check the strain distribution, however, equation (3.27) and equation (3.28) can be solved simultaneously for a_1 and b_1 when composite, fiber, and matrix properties are known. The ratio of the fiber strain to the matrix strain can then be found. For example, using the measured properties of an E-glass/epoxy composite [9],

$$\begin{aligned} &E_1 = 5.05\times10^6 \text{ psi} \quad (34.82 \text{ GPa}); \quad v_m = 0.55 \\ &E_2 = 1.53\times10^6 \text{ psi} \quad (10.55 \text{ GPa}); \quad v_f = 0.45 \\ &E_{f1} = E_{f2} = 10.5\times10^6 \text{ psi} \quad (72.4 \text{ GPa}) \\ &E_m = 0.55\times10^6 \text{ psi} \quad (3.79 \text{ GPa}) \end{aligned} \tag{3.29}$$

we find that $a_1 = 2.0884$, $b_1 = 0.1093$, $a_1/b_1 = \bar{\sigma}_{f1}/\bar{\sigma}_{m1} = 19.1$, and $\bar{\varepsilon}_{f1}/\bar{\varepsilon}_{m1} = 1.00$. Thus, the assumption of equal strains, which led to equation (3.23), is valid

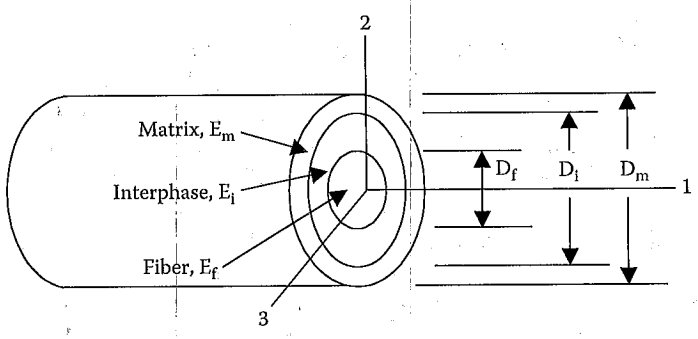

FIGURE 3.7
Self-consistent RVE for three-phase composite, including fiber, matrix, and fiber/matrix interphase.

for this material, as it apparently is for other composites. The strain energy approach will be used again in the next section to check the validity of an assumption leading to the equation for the transverse modulus.

EXAMPLE 3.3
As shown in figure 3.7, an RVE for a three-phase unidirectional composite is approximated by three concentric cylinders representing the fiber, the matrix, and the fiber/matrix interphase. The fiber/matrix interphase is a region surrounding the fiber, which has different properties from either the fiber or the matrix. Interphase regions may be created during processing as a result of interactions between the matrix materials and either the fiber material or a fiber-sizing material. Since the geometrical features of this model are not associated with any specific fiber-packing array geometry, it has been referred to as a "self-consistent model" [8]. Assuming that the three materials are linear elastic, isotropic, and securely bonded together, derive the micromechanics equation for the longitudinal modulus, E_1, of the composite.

Solution. The three constituent materials are arranged in parallel; so static equilibrium requires that the total resultant force on the composite must equal the sum of the forces acting on the three materials. Accordingly, the rule of mixtures for longitudinal composite stress in equation (3.19) applies here, with the addition of a third term representing the interphase, as denoted by the subscript i

$$\bar{\sigma}_{c1} = \bar{\sigma}_f \upsilon_f + \bar{\sigma}_m \upsilon_m + \bar{\sigma}_i \upsilon_i$$

Now supplementing equation (3.20) with a similar stress–strain relationship for the interphase material and extending the assumption of equal strains

in the constituents (eq. [3.22]) to the interphase material as well, we get another rule of mixtures:

$$E_1 = E_f \upsilon_f + E_m \upsilon_m + E_i \upsilon_i = E_f \left(\frac{D_f^2}{D_m^2} \right) + E_m \left(\frac{D_m^2 - D_i^2}{D_m^2} \right) + E_i \left(\frac{D_i^2 - D_f^2}{D_m^2} \right)$$

where the diameters D_f, D_m, and D_i are defined in figure 3.7. Indeed, for a composite having any number of constituents, n, that are securely bonded together and arranged in parallel as in figure 3.7, the generalized rule of mixtures for the longitudinal composite modulus is

$$E_1 = \sum_{j=1}^{n} E_j \upsilon_j$$

where E_j and υ_j are the modulus and volume fraction of the jth constituent, respectively and $j = 1, 2, \ldots, n$.

3.2.2 Transverse Modulus

If the RVE in figure 3.5(a) is subjected to a transverse normal stress, $\bar{\sigma}_{c2}$, as shown in figure 3.5(c), the response is governed by the effective transverse modulus, E_2. Geometric compatibility requires that the total transverse composite displacement, $\bar{\delta}_{c2}$, must equal the sum of the corresponding transverse displacements in the fiber, $\bar{\delta}_{f2}$, and the matrix, $\bar{\delta}_{m2}$:

$$\bar{\delta}_{c2} = \bar{\delta}_{f2} + \bar{\delta}_{m2} \tag{3.30}$$

It follows from the definition of normal strain that

$$\bar{\delta}_{c2} = \bar{\varepsilon}_{c2} L_2, \quad \bar{\delta}_{f2} = \bar{\varepsilon}_{f2} L_f, \quad \bar{\delta}_{m2} = \bar{\varepsilon}_{m2} L_m \tag{3.31}$$

and equation (3.30) now becomes

$$\bar{\varepsilon}_{c2} L_2 = \bar{\varepsilon}_{f2} L_f + \bar{\varepsilon}_{m2} L_m \tag{3.32}$$

Since the dimensions of the RVE do not change along the 1 direction, the length fractions must be equal to the volume fractions, and equation (3.32) can be rearranged to get the rule of mixtures for transverse strains:

$$\bar{\varepsilon}_{c2} = \bar{\varepsilon}_{f2} \upsilon_f + \bar{\varepsilon}_{m2} \upsilon_m \tag{3.33}$$

The 1-D Hooke's laws for this case are

$$\bar{\sigma}_{c2} = E_2\bar{\varepsilon}_{c2}, \quad \bar{\sigma}_{f2} = E_{f2}\bar{\varepsilon}_{f2}, \quad \bar{\sigma}_{m2} = E_m\bar{\varepsilon}_{m2} \tag{3.34}$$

where the Poisson strains have again been neglected. As with the longitudinal case, the inclusion of such strains would lead to a much more complex state of stress due to the mismatch in Poisson strains at the interface [10,11]. This is another example of the difference between a mechanics of materials solution and a more rigorous theory of elasticity solution. Combining equation (3.34) and equation (3.33), we get

$$\frac{\bar{\sigma}_{c2}}{E_2} = \frac{\bar{\sigma}_{f2}}{E_{f2}}\upsilon_f + \frac{\bar{\sigma}_{m2}}{E_m}\upsilon_m \tag{3.35}$$

If we assume that the stresses in the composite, matrix, and fiber are all equal, equation (3.35) reduces to the "inverse rule of mixtures" for the transverse modulus:

$$\frac{1}{E_2} = \frac{\upsilon_f}{E_{f2}} + \frac{\upsilon_m}{E_m} \tag{3.36}$$

From the RVE in figure 3.5, it would seem that the assumption of equal stresses is valid because equilibrium requires that the forces must be equal for the series arrangement, and both fiber and matrix blocks have equal areas normal to the 2 direction. In the actual composite, however, the fiber-packing arrangement is such that the forces and areas for the fiber and matrix are not necessarily equal, and we will use a strain energy approach to show that the resulting stresses are not equal. Thus, equation (3.36) is generally not acceptable for design use. As shown in figure 3.5(a), equation (3.36) gives the same result as equation (3.23) at the extreme values of fiber volume fraction, (i.e., $\upsilon_f = 0$ and $\upsilon_f = 1.0$), but it predicts significant improvement in the transverse modulus only at high fiber volume fractions. This turns out to be the correct trend, but, as shown in section 3.5, the experimental data falls well above the curve.

As with the longitudinal case, the strain energy approach provides additional insight into the micromechanics of the transverse loading case. We now express the fiber and matrix strains in terms of the composite strain:

$$\bar{\varepsilon}_{f2} = a_2\bar{\varepsilon}_{c2}, \quad \bar{\varepsilon}_{m2} = b_2\bar{\varepsilon}_{c2} \tag{3.37}$$

where a_2 and b_2 are constants. Substitution of equation (3.37) in the compatibility expression, equation (3.33) yields

$$a_2\upsilon_f + b_2\upsilon_m = 1 \tag{3.38}$$

By substituting equation (3.37) and equation (3.34) in equations analogous to equation (3.25) for the transverse loading case and the strain energy expression, equation (3.24), we find that

$$E_2 = a_2^2E_{f2}\upsilon_f + b_2^2E_m\upsilon_m \tag{3.39}$$

where the strain energy due to the Poisson strain mismatch at the interface has again been neglected. It is important to note that we did not assume equal stresses in the fibers and the matrix in order to get equation (3.39). Using the properties for the E-glass/epoxy given in equation (3.29) and solving equation (3.38) and equation (3.39) simultaneously, we find that $a_2 = 0.432$, $b_2 = 1.465$, the strain ratio $a_2/b_2 = \bar{\varepsilon}_{f2}/\bar{\varepsilon}_{m2} = 0.295$, and the corresponding stress ratio is $\bar{\sigma}_{f2}/\bar{\sigma}_{m2} = 5.63$. Thus, the assumption of equal stresses in fibers and matrix, which led to equation (3.36), is not justified for this material and is apparently not valid for most other composites as well. More accurate alternative design equations for the transverse modulus will be discussed later.

3.2.3 Shear Modulus and Poisson's Ratio

The major Poisson's ratio, ν_{12}, and the in-plane shear modulus, G_{12}, are most often used as the two remaining independent elastic constants for the orthotropic lamina. The major Poisson's ratio, which is defined as

$$\nu_{12} = -\frac{\bar{\varepsilon}_{c2}}{\bar{\varepsilon}_{c1}} \tag{3.40}$$

when the only nonzero stress is a normal stress along the 1 direction, can be found by solving the geometric compatibility relationships associated with both the 1 and the 2 directions. The result is another rule of mixtures formulation:

$$\nu_{12} = \nu_{f12}\upsilon_f + \nu_m\upsilon_m \tag{3.41}$$

where ν_{f12} is the major Poisson's ratio of fiber and ν_m the Poisson's ratio of matrix.

Equation (3.41) is generally accepted as being sufficiently accurate for design purposes. As in the case for the longitudinal modulus, the geometric compatibility relationships leading to the solution are valid.

The effective in-plane shear modulus is defined as (fig. 3.5[d])

$$G_{12} = \frac{\bar{\sigma}_{c12}}{\bar{\gamma}_{c12}} \tag{3.42}$$

where $\bar{\sigma}_{c12}$ is the average composite shear stress in the 12 plane and $\gamma_{c12} = 2\bar{\varepsilon}_{c12}$, the average engineering shear strain in the 12 plane.

An equation for the in-plane shear modulus can be derived using an approach similar to that which was used for the transverse modulus. That is, geometric compatibility of the shear deformations, along with the assumption of equal shear stresses in fibers and matrix, leads to another inverse rule of mixtures:

$$\frac{1}{G_{12}} = \frac{v_f}{G_{f12}} + \frac{v_m}{G_m} \tag{3.43}$$

where G_{f12} is the shear modulus of fiber in the 12 plane and G_m = shear modulus of matrix.

As we might expect, this equation is not very accurate because the shear stresses are not equal as assumed. A strain energy approach similar to that used in section 3.2.2 can be used here to show that the shear stresses are in fact not equal. As with the transverse modulus, we need to find better equations for estimating the in-plane shear modulus. Such equations will be discussed in the following sections.

EXAMPLE 3.4

The constituent materials in the composite described in example 3.1 and example 3.2 have the properties $E_{f1} = 32.0 \times 10^6$ psi (220 GPa), $E_{f2} = 2.0 \times 10^6$ psi (13.79 GPa), and $E_m = 0.5 \times 10^6$ psi (3.45 GPa). Estimate the longitudinal and transverse moduli of the composite. Given these fiber and matrix materials, what are the maximum possible values of E_1 and E_2?

Solution. The longitudinal modulus is given by equation (3.23)

$$E_1 = (32 \times 10^6)0.506 + (0.5 \times 10^6)0.482 = 16.43 \times 10^6 \text{ psi} (113 \text{ GPa})$$

The transverse modulus is roughly estimated by equation (3.36):

$$E_2 = \frac{1}{\frac{0.506}{32 \times 10^6} + \frac{0.482}{0.5 \times 10^6}} = 0.82 \times 10^6 \text{ psi} \ (5.65 \text{ GPa})$$

As expected, the composite is highly anisotropic, with $E_1 >> E_2$. If the composite has the theoretical maximum fiber volume fraction of 0.907 for a close-packed triangular array (eq. [3.13]), the corresponding composite properties are still highly anisotropic, with $E_1 = 29 \times 10^6$ psi (200 GPa) and $E_2 = 1.56 \times 10^6$ psi (10.75 GPa). Note that even with this maximum fiber content, the transverse modulus is still very low. Thus, some transverse reinforcement is usually necessary in practical applications. Note also that the longitudinal modulus of the graphite/epoxy composite is now about the same as the modulus of steel, but the density of the composite is only about 20% of the density of steel. Composites typically have much greater stiffness-to-weight ratios than conventional metallic structural materials.

EXAMPLE 3.5

For longitudinal loading of the composites in example 3.4, compare the stresses in the fiber and matrix materials. Compare the strain energy stored in the fibers with that stored in the matrix.

Solution. From equation (3.20) and equation (3.22), the ratio of fiber stress to matrix stress is

$$\frac{\bar{\sigma}_{f1}}{\bar{\sigma}_{m1}} = \frac{E_{f1}\bar{\varepsilon}_{f1}}{E_m\bar{\varepsilon}_{m1}} = \frac{E_{f1}}{E_m} = \frac{32.0}{0.5} = 64.0$$

Thus, the fiber carries most of the stress since the fiber modulus is always higher than the matrix modulus. From equation 3.25(b), equation 3.25(c), and equation (3.22), the ratio of fiber strain energy to matrix strain energy is

$$\frac{U_f}{U_m} = \frac{E_{f1}v_f}{E_m v_m} = \frac{32.0(0.506)}{0.5(0.482)} = 67.0$$

that is almost the same as the stress ratio. If the composite had the maximum possible fiber volume fraction of 0.907, the stress ratio would remain the same since it is independent of the fiber volume fraction. The strain energy ratio would increase dramatically to 624, however, since it is proportional to the ratio of fiber volume fraction to the matrix volume fraction.

3.3 Improved Mechanics of Materials Models

As shown in the previous section, the elementary mechanics of materials models for E_1 and ν_{12} are good enough for design use. The corresponding models for E_2 and G_{12} are of questionable value, however, because they are based on invalid assumptions, and agreement with experimental results is

generally poor. We will now discuss several refinements of the elementary mechanics of materials models.

Due to the simplified RVE that was used for the elementary mechanics of materials approach (fig. 3.5), the resulting equations were not tied to any particular fiber-packing geometry. Since the results for E_1 and v_{12} were so favorable, we can conclude that those properties must be essentially independent of fiber-packing geometry. By the same reasoning, it appears that E_2 and G_{12} may be more sensitive to fiber-packing geometry. Thus, the assumption of a specific fiber-packing array is one possible refinement of the models. Although real composites have random-packing arrays, the assumption of a regular array is a logical simplification if we are to have any hope of developing simple design equations. Such an assumption allows us to use simple relations among fiber size, spacing, and volume fraction. Hopkins and Chamis [12] have developed a refined model for transverse and shear properties based on a square fiber-packing array and a method of dividing the RVE into subregions. The following derivation is adapted from ref. [12].

A square array of fibers is shown in figure 3.1, and the RVE for such an array is shown in figure 3.8. The RVE is easily divided into subregions for more detailed analysis if we convert to a square fiber having the same area as the round fiber. The equivalent square fiber shown in figure 3.8 must then have the dimension

$$s_f = \sqrt{\frac{\pi}{4}}d \tag{3.44}$$

and from equation (3.10), the size of the RVE is

$$s = \sqrt{\frac{\pi}{4v_f}}d \tag{3.45}$$

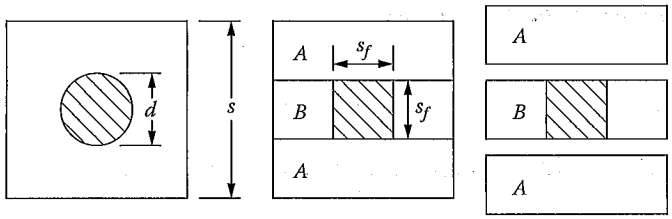

FIGURE 3.8
Division of RVE into subregions based on square fiber having equivalent fiber volume fraction.

The RVE is divided into subregions A and B, as shown in figure 3.8. In order to find the effective transverse modulus for the RVE, we first subject the series arrangement of fiber and matrix in subregion B to a transverse normal stress. Following the procedure of section 3.2.2, the effective transverse modulus for this subregion, E_{B2}, is found to be

$$\frac{1}{E_{B2}} = \frac{1}{E_{f2}}\frac{s_f}{s} + \frac{1}{E_m}\frac{s_m}{s} \tag{3.46}$$

where the matrix dimension is $s_m = s - s_f$. From equation (3.44) and equation (3.45), it is seen that

$$\frac{s_f}{s} = \sqrt{v_f} \quad \text{and} \quad \frac{s_m}{s} = 1 - \sqrt{v_f} \tag{3.47}$$

so that equation (3.46) now becomes

$$E_{B2} = \frac{E_m}{1 - \sqrt{v_f}(1 - E_m/E_{f2})} \tag{3.48}$$

The parallel combination of subregions A and B is now loaded by a transverse normal stress and the procedure of section 3.2.1 is followed in order to find the effective transverse modulus of the RVE. The result, of course, is the rule of mixtures analogous to equation (3.21)

$$E_2 = E_{B2}\frac{s_f}{s} + E_m\frac{S_m}{s} \tag{3.49}$$

Substitution of equation (3.47) and equation (3.48) in equation (3.49) then gives the final result,

$$E_2 = E_m\left[\left(1 - \sqrt{v_f}\right) + \frac{\sqrt{v_f}}{1 - \sqrt{v_f}(1 - E_m/E_{f2})}\right] \tag{3.50}$$

A similar result may be found for G_{12}. The detailed derivation in ref. [12] also includes the effect of a third phase, a fiber/matrix interphase material, which is assumed to be an annular volume surrounding the fiber. Such interphase regions exist in many metal matrix [12] and polymer matrix [13] composites. When the fiber diameter is equal to the interphase diameter, the equation for E_2 in ref. [12] reduces to equation (3.50). The complete set of equations for effective moduli of the three-phase model is given in ref. [12]

In separate publications, Chamis [14,15] presented the so-called simplified micromechanics equations (SMEs), which are based on this same method of subregions, except that only the terms for subregion B (fig. 3.8) are retained. Thus, the SME for E_2 would be the same as that for E_{B2} in equation (3.48), and similar equations for the other effective moduli are given in refs. [14,15]. Also included in these references are tables of fiber and matrix properties to be used as input to the SME, and these tables are reproduced here in table 3.1 and table 3.2. It is important to note that in such tables the transverse fiber modulus, E_{f2}, and the longitudinal fiber shear modulus, G_{f12}, are not actually measured but are inferred by substitution of measured composite properties and matrix properties in the SME. The inferred properties show that fibers such as carbon and aramid are highly anisotropic, whereas glass and boron are essentially isotropic. Similar back-calculations of anisotropic fiber properties using other analytical models have been reported by Kriz and Stinchcomb [16] and by Kowalski [17]. More recently, direct measurement of fiber transverse moduli has been reported by Kawabata [18]. Kawabata's measurements, based on transverse diametral compression of single carbon and aramid fibers, show even greater anisotropy than the inferred properties in table 3.1 and table 3.2. However, Caruso and Chamis [19] have shown that the SME and the corresponding tables of properties give results that agree well with 3-D finite element models, as shown in figure 3.9. Since the SME for E_1 and ν_{12} are the same as equation (3.23) and equation (3.41), respectively, this comparison provides further evidence of the validity of those equations.

Another set of equations for E_2 and G_{12} has been derived by Spencer [20] who used a square array model that included the effects of the strain concentration at points of minimum clearance between fibers in the RVE. Spencer's equation is

$$\frac{M_c}{M_m} = \frac{\Gamma - 1}{\Gamma} + \frac{1}{k}\left[\frac{\pi}{2} + \frac{2\Gamma}{\sqrt{\Gamma^2 - k^2}} \tan^{-1}\sqrt{\frac{\Gamma + k}{\Gamma - k}}\right] \tag{3.51}$$

where $M_c = E_2$, $M_m = E_m$, and $k = 1 - E_m/E_{f2}$ for the transverse modulus equation and $M_c = G_{12}$, $M_m = G_m$, and $k = 1 - G_m/G_{f12}$ for the longitudinal shear modulus equation. The parameter $\Gamma = s/d$ in both the equations. Spencer also suggests that Γ can be accurately approximated for a variety of packing geometries over the full range of fiber volume fractions, v_f, by the equation

$$\Gamma = \frac{1}{\sqrt{\left(1.1v_f^2 - 2.1v_f + 2.2\right)v_f}} \tag{3.52}$$

Spencer does not include a table of suggested properties for use with these equations.

TABLE 3.1
Fiber Properties

Properties	Units	Boron	HMS	AS	T300	KEV	S-G	E-G
Number of fibers per end	—	1	10000	10000	3000	580	204	204
Fiber diameter	in.	0.0056	0.0003	0.0003	0.0003	0.00046	0.00036	0.00036
Density	lb/in.^{3}	0.095	0.070	0.063	0.064	0.053	0.090	0.090
Longitudinal modulus	10^6 psi	58	55.0	31.0	32.0	22	12.4	10.6
Transverse modulus	10^6 psi	58	0.90	2.0	2.0	0.6	12.4	10.6
Longitudinal shear modulus	10^6 psi	24.2	1.1	2.0	1.3	0.42	5.17	4.37
Transverse shear modulus	10^6 psi	24.2	0.7	1.0	0.7	0.22	5.17	4.37
Longitudinal Poisson's ratio	—	0.20	0.20	0.20	0.20	0.35	0.20	0.22
Transverse Poisson's ratio	—	0.20	0.25	0.25	0.25	0.35	0.20	0.22
Heat capacity	btu/lb/°F	0.31	0.20	0.20	0.22	0.25	0.17	0.17
Longitudinal heat conductivity	btu/h/ft²/°F/in	22	580	580	580	1.7	21	7.5
Transverse heat conductivity	btu/h/ft²/°F/in	22	58	58	58	1.7	21	7.5
Longitudinal thermal expansion coefficient	10^{-6} in./in./°F	2.8	−0.55	−0.55	−0.55	−2.2	2.8	2.8
Transverse thermal expansion coefficient	10^{-6} in./in./°F	2.8	5.6	5.6	5.6	30	2.8	2.8
Longitudinal tensile strength	ksi	600	250	350	350	400	600	400
Longitudinal compression strength	ksi	700	200	260	300	75	—	—
Shear strength	ksi	100	—	—	—	—	—	—

Note: Transverse, shear, and compression properties are estimates inferred from corresponding composite properties.

Source: From Chamis, C.C. 1987. In: Weeton, J.W., Peters, D.M., Thomas, K.L. eds. *Engineers' Guide to Composite Materials*. ASM International, Materials Park, OH. With permission.

TABLE 3.2

Matrix Properties

Parameters	Units	LM	IMLS	IMHS	HM	Polyimide	PMR
Density	lb/in.^{3}	0.042	0.046	0.044	0.045	0.044	0.044
Modulus	10^6 psi	0.32	0.50	0.50	0.75	0.50	0.47
Shear modulus	10^6 psi	—	—	—	—	—	—
Poisson's ratio	—	0.43	0.41	0.35	0.35	0.35	0.36
Heat capacity	btu/lb/°F	0.25	0.25	0.25	0.25	0.25	0.25
Heat conductivity	btu/h/ft^2/°F/in.	1.25	1.25	1.25	1.25	1.25	1.25
Thermal expansion coefficient	10^{-6} in./in./°F	57	57	36	40	20	28
Diffusivity	10^{-10} in.^{2}/s	0.6	0.6	0.6	0.6	0.6	0.6
Moisture expansion coefficient	in./in./M	0.33	0.33	0.33	0.33	0.33	0.33
Tensile strength	ksi	8	7	15	20	15	8
Compression strength	ksi	15	21	35	50	30	16
Shear strength	ksi	8	7	13	15	13	8
Tensile fracture strain	in./in. (%)	8.1	1.4	2.0	2.0	2.0	2.0
Compressive fracture strain	in./in. (%)	15	4.2	5.0	5.0	4.0	3.5
Shear fracture strain	in./in. (%)	10	3.2	3.5	4.0	3.5	5.0
Air heat conductivity	btu/h/ft^2/°F/in.	0.225	0.225	0.225	0.225	0.225	0.225
Glass transition temperature (dry)	°F	350	420	420	420	700	700

Note: LM = low modulus; IMLS = intermediate modulus low strength; IMHS = intermediate modulus high strength; HM = high modulus. Thermal, hygral, compression, and shear properties are estimates only; $G_m = E_m/2(1 + \nu_m)$.

Source: From Chamis, C.C., 1987, In: Weeton, J.W., Peters, D.M., and Thomas, K.L. eds. *Engineers' Guide to Composite Materials*. ASM International, Materials Park, OH. With permission.

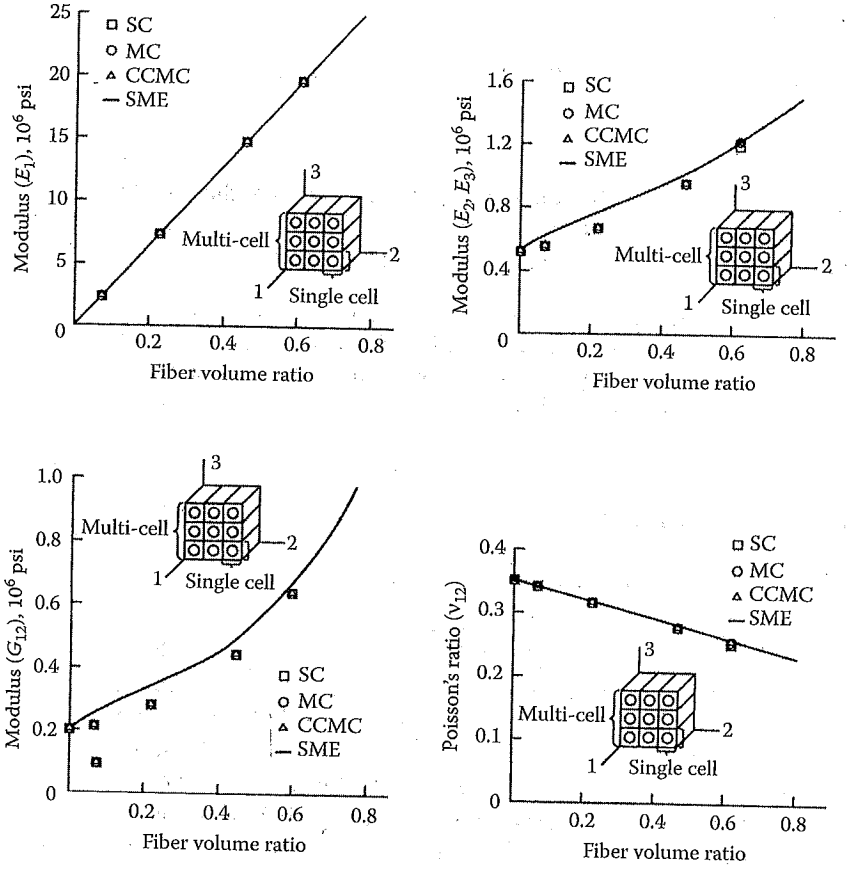

FIGURE 3.9

Comparison of 3-D finite element results for lamina elastic constants with predictions from SMEs for carbon/epoxy. (From Caruso, J.J. and Chamis, C.C. 1986. *Journal of Composites Technology and Research*, 8(3), 77–83. With permission.)

EXAMPLE 3.6

For the composite in example 3.4, compare transverse modulus values calculated by the inverse rule of mixtures (eq. [3.36]), the method of subregions (eq. [3.50]), and Spencer's equation (eq. [3.51]).

Solution. *The results from equation (3.36),* as previously calculated in example 3.4, are:

$$E_2 = 0.82 \times 10^6 \text{ psi } (5.65 \text{ GPa})$$

Equation (3.50):

$$E_2 = 0.9 \times 10^6 \text{ psi } (6.2 \text{ GPa})$$

Equation (3.51):

First estimate $\Gamma = 1.18$ from equation (3.52). Note that the actual value of Γ from example 3.2 is $\Gamma = s/d = 0.000623/0.0005 = 1.25$. Using $\Gamma = 1.18$ in equation (3.51), we have $E_2 = 0.98 \times 10^6$ psi (6.76 GPa).

As previously mentioned, the inverse rule of mixtures prediction for the transverse modulus is considerably lower than measured values. The higher values given by the method of subregions and Spencer's equation are more accurate. Further discussion on this will follow in the next section.

3.4 Elasticity Models

The theory of elasticity approach to micromechanical modeling begins in the same way as the mechanics of materials approach, by selecting the RVE and then subjecting the RVE to uniform stress or displacement at the boundary. The two approaches differ substantially in the solution of the resulting boundary value problem, however. The equations of elasticity must be satisfied at every point in the model, and no simplifying assumptions are made regarding the stress or strain distributions as in the mechanics of materials approach. Fiber-packing geometry is generally specified in the elasticity approach. A variety of closed-form and numerical solutions of the governing equations of elasticity have been reported in the literature [1–4], and a complete review of the work in this area is beyond the scope of this book. However, the stress equilibrium equations and the strain-displacement relations from elasticity theory are derived in Appendices A and B, respectively. The objective here is to discuss several representative numerical and closed-form solutions in order to show what additional knowledge of micromechanical behavior can be obtained from the more rigorous elasticity approach.

Numerical solutions of the governing elasticity equations are often necessary for complex structural geometries such as those found in the RVEs used in micromechanics models. For example, Adams and Doner [21] used a finite difference solution to determine the shear modulus G_{12} for a rectangular array of fibers. A displacement boundary value problem was solved for one quadrant of the RVE, as shown in figure 3.10. Note that Adams and Doner use the z-axis to define the fiber direction, whereas the x and y axes correspond to the transverse directions. The displacement

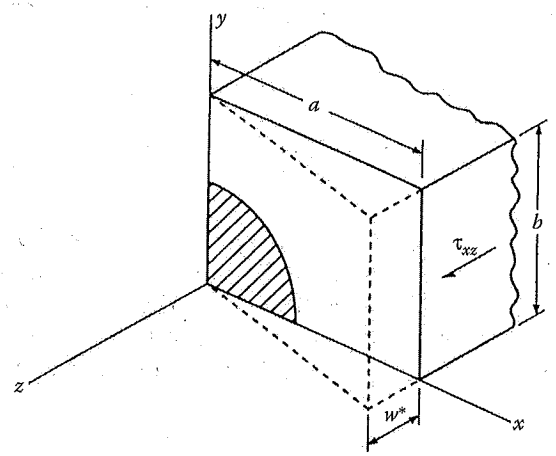

FIGURE 3.10
One quadrant of an RVE from Adams and Doner elasticity solution for shear modulus G_{12}. (*From Adams and Doner* [21]. *Reproduced by permission of Technomic Publishing Co.*)

components u, v, and w correspond to the x, y, and z axes, respectively. The imposed displacement w^* along $x = a$ causes a displacement field of the form

$$u = v = 0, \quad w = w(x, y) \tag{3.53}$$

From the strain-displacement equations (Appendix B) and Hooke's law, the only nonvanishing stress components are

$$\tau_{zx} = G\frac{\partial w}{\partial x} \quad \text{and} \quad \tau_{zy} = G\frac{\partial w}{\partial y} \tag{3.54}$$

where the shear modulus, G, may be either the fiber or matrix property, depending on the coordinates x and y. Isotropic behavior was assumed for both fiber and matrix materials. Substitution of equations (3.54) in the only nontrivial stress equilibrium equation (Appendix A) yielded the governing partial differential equation

$$G\left[\frac{\partial^2 w}{\partial x^2} + \frac{\partial^2 w}{\partial y^2}\right] = 0 \tag{3.55}$$

which was solved subject to the displacement boundary conditions

$$w(0,y)=0, \quad w(a,y)=w^*$$
$$G\frac{\partial w}{\partial y}=0 \quad \text{along} \quad y=0 \quad \text{and} \quad y=b \tag{3.56}$$

and continuity conditions at the fiber/matrix interface by using a finite difference scheme. The solution yielded the values of the displacements $w(x,y)$ at each node of the finite difference grid. Stresses were found by substituting these displacements in the finite difference forms of equation (3.54), and the effective shear modulus was then determined from

$$G_{xz}=\frac{\bar{\tau}_{xz}}{w^*/a} \tag{3.57}$$

where $\bar{\tau}_{xz}$ is the average shear stress along $x=a$. A similar boundary value problem for shear along $y=b$ yields the associated shear modulus G_{yz}. Typical results are shown in figure 3.11, where the ratio of the composite

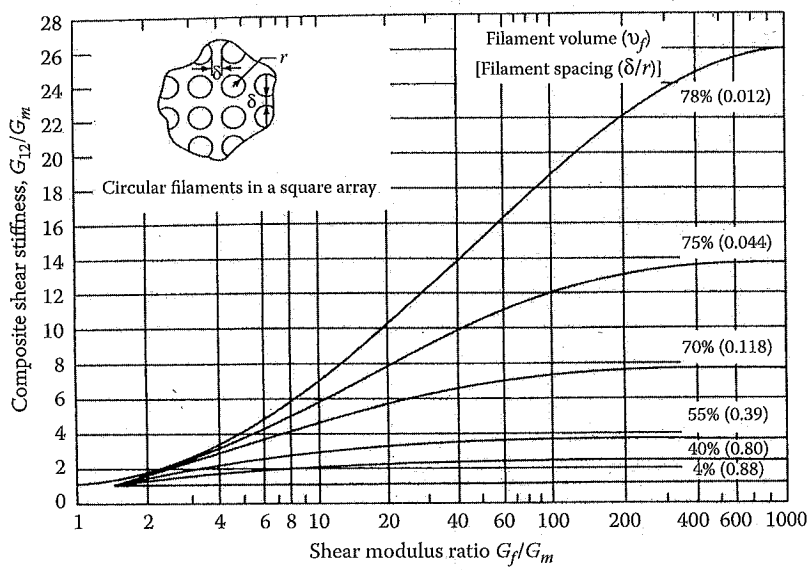

FIGURE 3.11
Normalized composite shear stiffness, G_{12}/G_m, vs. shear modulus ratio, G_f/G_m, for circular fibers in a square array. (From Adams, D.F. and Doner, D.R. 1967. *Journal of Composite Materials*, 1, 4–17. With Permission from Technomic Publishing Co.)

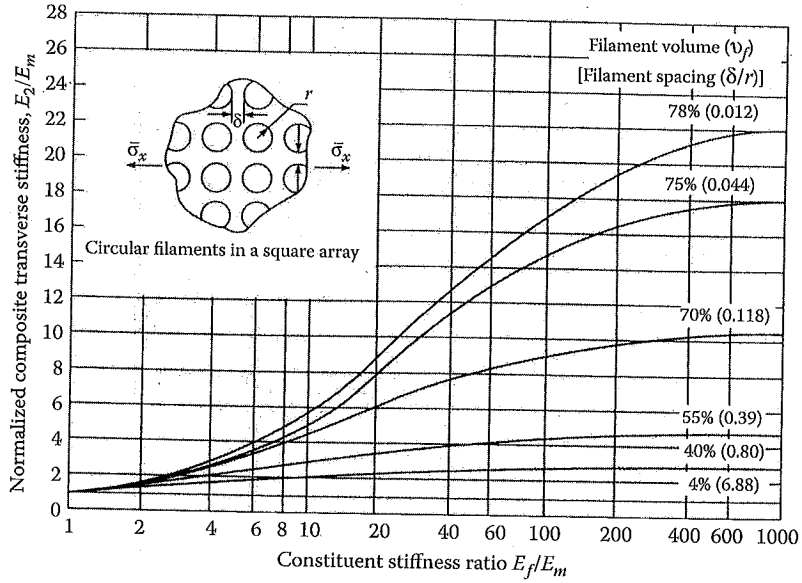

FIGURE 3.12
Normalized composite transverse stiffness, E_2/E_m, versus modulus ratio, E_f/E_m, for circular fibers in a square array. (Adams, D.F. and Doner, D.R. 1967. *Journal of Composite Materials*, 1, 152–164. With permission from Technomic Publishing Co.)

shear modulus to the matrix shear modulus is plotted versus the shear modulus ratio G_f/G_m for various fiber volume fractions.

In a separate paper Adams and Doner [22] used a similar approach to determine the transverse modulus E_2 and typical results are shown in figure 3.12. It is seen in figure 3.11 and figure 3.12 that the reinforcement effect for both G_{12} and E_2 only becomes significant for fiber volume fractions above about 50%, but that combinations of high fiber stiffness and high fiber volume fractions can significantly increase G_{12} and E_2. Unfortunately, these same combinations also generate very high stress concentration factors at the fiber/matrix interfaces, as shown in the same papers [21,22]. One of the advantages of the elasticity approach is that the complete stress and strain distributions in the RVE are generated, and the calculation of stress concentration factors is possible. One advantage of numerical solutions such as finite differences is the capability for analysis of complex geometries. For example, stiffness and stress concentration factors were also obtained for a variety of fiber cross-sectional shapes such as squares and ellipses in a rectangular array [21,22].

The previously mentioned finite element analysis of Caruso and Chamis [19] and Caruso [23] is another example of a numerical elasticity solution.

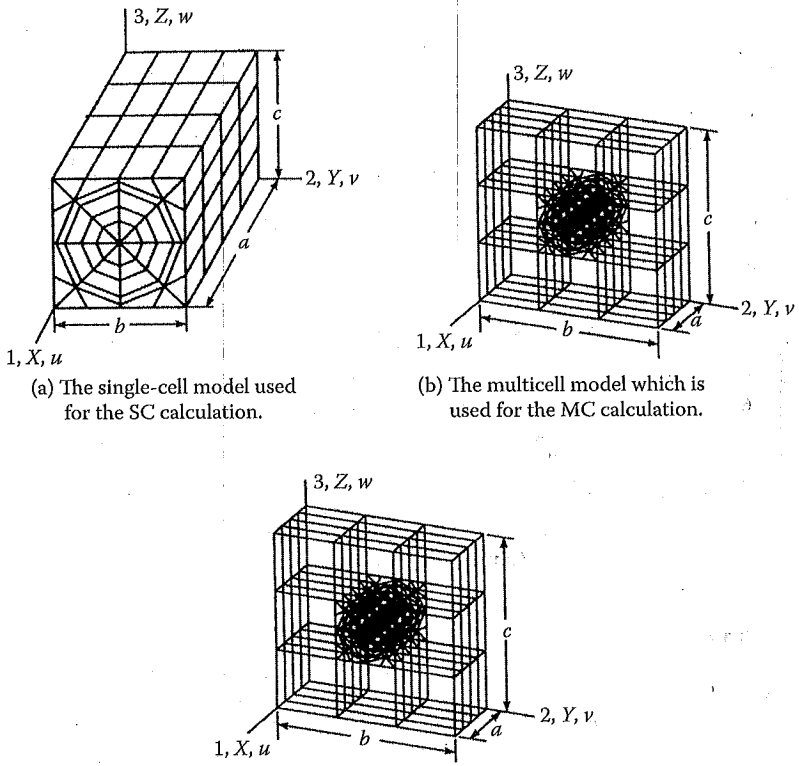

(a) The single-cell model used for the SC calculation.

(b) The multicell model which is used for the MC calculation.

(c) The multicell model which only the center cell is used for the CCMC calculation.

FIGURE 3.13
3-D finite element models of RVEs. (From Caruso, J.J. and Chamis, C.C. 1986. *Journal of Composites Technology and Research*, 8(3), 77–83. Copyright, ASTM. With permission.)

In this case, a single-cell (SC) finite element model was developed from 192 3-D isoparametric brick elements (fig. 3.13). This SC model was then used as a building block for a multicell (MC) model consisting of nine SC models in a 3 × 3 array (fig. 3.9). A third model (CCMC) used only the center cell in the nine-cell MC model for the calculations. Boundary and load conditions were consistent with those used for the previously discussed SME mechanics of materials solutions, so that the finite element results could be compared with the SME results. For example, equation (3.57) and similar equations were used to determine stiffnesses from finite element results. Material properties for AS graphite fibers in an intermediate-modulus-high-strength (IMHS) epoxy matrix were used (table 3.1 and table 3.2). Fibers were assumed to be orthotropic, whereas the matrix

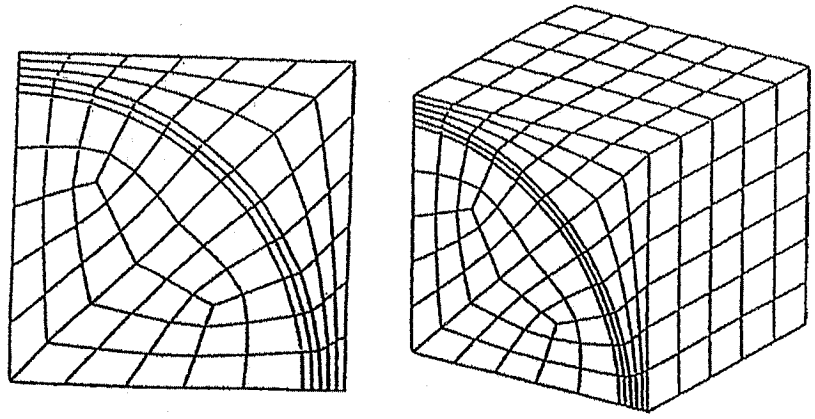

FIGURE 3.14
Examples of 2-D and 3-D finite element quarter domain micromechanics models. (From Finegan, I.C. and Gibson, R.F. 1997. In Farabee, T.M. ed. *Proceedings of ASME Noise Control and Acoustics Division*. NCA-Vol.24, pp. 127–138. With permission.)

was assumed to be isotropic. As shown in figure 3.9, the finite element results show good agreement with SME results.

As with the previously discussed finite difference approach used in references [21,22], the quarter domain model of a representative volume can also be analyzed by using finite elements. Typical 2-D and 3-D quarter domain finite element models are shown in figure 3.14 from ref. [24]. For example, in one study, 3-D finite element quarter domain models similar to the one in figure 3.14 were subjected to transverse normal loading as in figure 3.15, and the effect of model aspect ratio $L/(D/2)$ on the transverse modulus was determined, as shown in figure 3.16. This particular model included a fiber coating or interphase region between the fiber and the matrix (see example 3.3 for further discussion of the interphase). The transverse modulus was calculated by imposing a uniform displacement U_x along the edge $x = D/2$ and then using the calculated stresses from the finite element model to evaluate equation (3.58):

$$E_x = \frac{\bar{\sigma}_x}{\bar{\varepsilon}_x} = \frac{\int_V \sigma_x dV}{\int_V \varepsilon_x dV} \tag{3.58}$$

where $\bar{\sigma}_x$ = average stress acting along $x = D/2$ in figure 3.15,

$$\bar{\varepsilon}_x = \frac{U_x}{(D/2)} = \text{average strain along } x = D/2$$

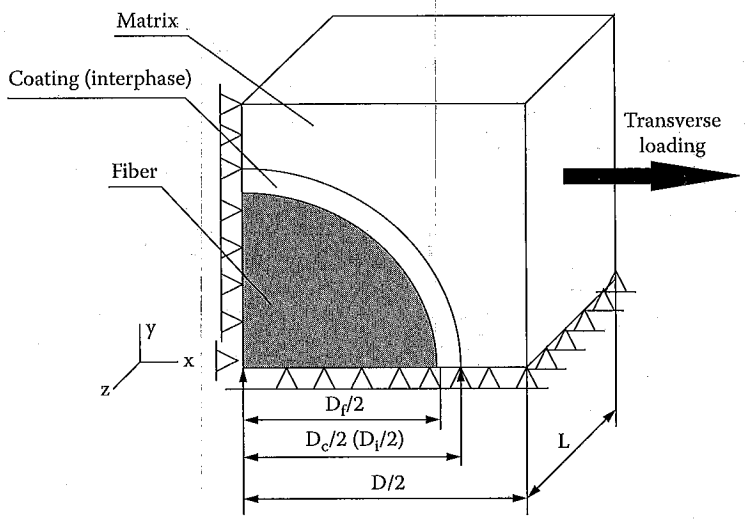

FIGURE 3.15
Quarter domain of RVE under transverse normal loading. (From Finegan, I.C. and Gibson, R.F. 1998. *Journal of Vibration and Acoustics*, 120(2), 623–627. With permission.)

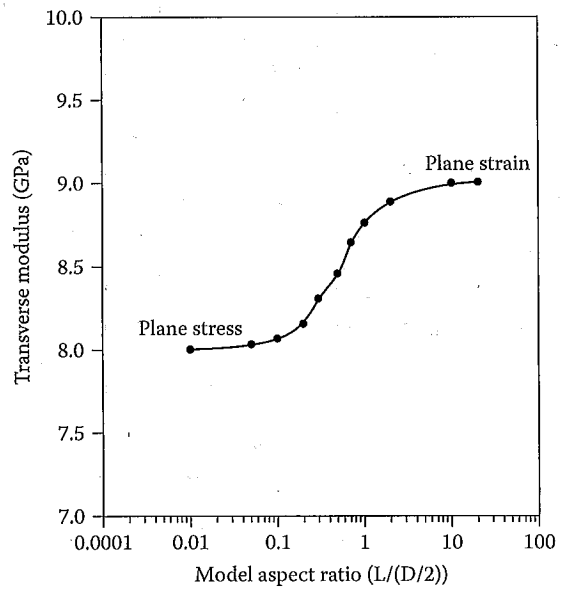

FIGURE 3.16
Variation of transverse modulus with model aspect ratio for graphite/epoxy composite from 3-D finite element models. (From Finegan, I.C. and Gibson, R.F. 1998. *Journal of Vibration and Acoustics*, 120(2), 623–627. With permission.)

where
$D/2$ = dimension defined in figure 3.15
U_x = imposed displacement along $x = D/2$
L = length of model along x, the fiber direction
V = volume

It is seen from figure 3.16 that the transverse modulus varies from a minimum value for low-model aspect ratios to a maximum for high-model aspect ratios. It was also shown that the low-model aspect ratio results from 3-D models coincided with the results obtained by using 2-D plane stress elements (i.e., with longitudinal stress $\sigma_z = 0$), while the high-model aspect ratio results from 3-D models coincided with the results obtained by using 2-D plane strain elements (i.e., with longitudinal strain $\varepsilon_z = 0$). For a unidirectional composite having continuous fibers oriented along the z direction, the plane strain condition is more realistic than the plane stress condition. The importance of this observation is that 2-D plane strain elements can be used for these types of models instead of 3-D elements, and this leads to significant reductions in the number of elements and the corresponding computation time.

As an example of a closed-form elasticity solution, Whitney and Riley [8] used axisymmetric airy stress functions to solve for the stresses and strains in a so-called "self-consistent" model having a single isotropic fiber embedded in a concentric cylinder of isotropic matrix material. The cylindrical geometry of the self-consistent model is such that the model is not associated with any specific fiber-packing geometry. The resulting micromechanical stresses and strains were then used in energy balance equations similar to equation (3.24) and equation (3.25) to solve for E_1 and E_2. The equation for E_1 reduces to the rule of mixtures when the Poisson's ratio of the fiber is equal to that of the matrix. The additional term is due to the mismatch in Poisson strains at the fiber/matrix interface (recall that this term was neglected in equation [3.24] and equation [3.25]). Predictions showed good agreement with experimental data for boron/epoxy. In a later paper, Whitney extended the analysis to include anisotropic, transversely isotropic fibers [26].

Another closed-form micromechanical elasticity approach, the method of cells, was developed by Aboudi [27]. A representative cell consisting of a square fiber embedded in a square of matrix material was divided into four subcells. Equilibrium equations were then solved subject to continuity of displacements and tractions at the interfaces between the subcells and between neighboring cells on an average basis, along with the assumption of linear variations of displacements in each subcell. The equations are too lengthy to present here, but excellent agreement was

observed with the experimental data on graphite/epoxy from ref. [16]. One advantage of this approach is that it yields not only the in-plane lamina properties, but also the through-the-thickness properties such as G_{23} and ν_{23}.

Paul [28] obtained closed-form solutions for the bounds on the transverse modulus of a fiber composite (or the Young's modulus of an isotropic-particle-reinforced composite) by using a variational approach. By applying the theorem of minimum complementary energy to the situation where the composite is subjected to a uniaxial normal stress, Paul found the lower bound on E_2 to be the inverse rule of mixtures (eq. [3.36]). The application of the theorem of minimum potential energy to the situation where the composite is subjected to a simple extensional strain gave the upper bound on E_2, which reduces to the rule of mixtures (eq. [3.23]) when the Poisson's ratios of fiber and matrix materials are taken to be the same.

The bounds derived by Paul [28] are independent of packing geometry and are referred to as the elementary bounds. Thus, it should be no surprise that the bounds are very far apart, as shown in figure 3.6. Tighter bounds require the specification of packing geometry. For example, Hashin and Rosen [29] applied the principles of minimum potential and complementary energy to fiber composites with hexagonal and random arrays. Detailed summaries of these and other related results have been reported by Hashin [1] and Christensen [3]. More recently, Torquato [30] has reviewed advances in the calculation of improved bounds on the effective properties of random heterogeneous media. Such improved bounds are determined by using statistical correlation functions to model the random variations in the microstructure. Since the fiber-packing geometry in composites is of a random nature, such bounds should be more realistic than the bounds that are based on some idealized fiber-packing array.

3.5 Semiempirical Models

In section 3.3, improved mechanics of materials models for prediction of E_2 and G_{12} were discussed. Another general approach to estimating these properties involves the use of semiempirical equations that are adjusted to match experimental results or elasticity results by the use of curve-fitting parameters. The equations are referred to as being "semiempirical" because, although they have terms containing curve-fitting parameters,

they also have some basis in mechanics. The most widely used semiempirical equations were developed by Halpin and Tsai [31]. The Halpin–Tsai equation for the transverse modulus is

$$\frac{E_2}{E_m} = \frac{1+\xi\eta v_f}{1-\eta v_f} \tag{3.59}$$

where

$$\eta = \frac{(E_f/E_m)-1}{(E_f/E_m+\xi)} \tag{3.60}$$

and ξ is the curve-fitting parameter, which is also a measure of the degree of reinforcement of the matrix by the fibers. The corresponding equation for G_{12} is obtained by replacing the Young's moduli E_2, E_f, and E_m in the above equations by the shear moduli G_{12}, G_f, and G_m, respectively. Note that the values for the curve-fitting parameter may be different for E_2 and G_{12}. Halpin and Tsai found that the value $\xi = 2$ gave an excellent fit to the finite difference elasticity solution of Adams and Doner [22] for the transverse modulus of a square array of circular fibers having a fiber volume fraction of 0.55. For the same material and fiber volume fraction, a value of $\xi = 1$ gave excellent agreement with the Adams and Doner solution for G_{12} [21].

Jones [11] shows that when $\xi = 0$, the Halpin–Tsai equation reduces to the inverse rule of mixtures (eq. [3.36]), whereas a value of $\xi = \infty$ yields the rule of mixtures (eq. [3.23]). Recall that Paul [28] proved that these equations also represent the bounds on E_2. Thus, the interpretation of the curve-fitting parameter, ξ, as a measure of the degree of fiber reinforcement has a theoretical basis. The use of the Halpin–Tsai equations in a variety of other applications and related empirical equations for estimating the curve-fitting parameter are discussed in more detail by Jones [11] and Halpin [4].

Tsai and Hahn [10] have proposed another semiempirical approach to calculating E_2 and G_{12}, that is based on the fact that the stresses in the fibers and the matrix are not equal under the corresponding loading conditions. Recall that the proof of such differences was demonstrated using a strain energy approach in section 3.2.2. The method involves the use of empirical "stress-partitioning parameters" in derivations paralleling those used for the elementary mechanics of materials models. For

example, the Tsai–Hahn equation for E_2 is found by introducing a stress-partitioning parameter, η_2, and using the relationship

$$\bar{\sigma}_{m2} = \eta_2 \bar{\sigma}_{f2} \tag{3.61}$$

in a derivation similar to that used for the elementary mechanics of materials model for E_2 in section 3.2.2. The derivation was also based on the assumption that a rule of mixtures for stress similar to equation (3.19) also held for the transverse direction (2 direction). Although such an assumption is obviously not consistent with the RVE configuration and the loading condition shown in figure 3.5(c), it would be valid for a real composite with fiber packing such as that shown in figure 3.2. The result of this derivation is

$$\frac{1}{E_2} = \frac{1}{\upsilon_f + \eta_2 \upsilon_m}\left[\frac{\upsilon_f}{E_f} + \frac{\eta_2 \upsilon_m}{E_m}\right] \tag{3.62}$$

Note that equation (3.62) reduces to the inverse rule of mixtures (eq. [3.36]) when the stress-partitioning parameter $\eta_2 = 1.0$. This is to be expected since equation (3.36) was based on the assumption that the stresses in the fiber and the matrix are the same. A similar equation can be derived for the shear modulus, G_{12}, as shown in ref. [10]. Figure 3.17 from ref. [10] shows

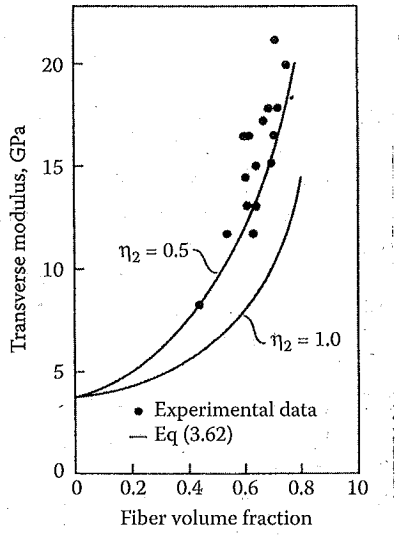

FIGURE 3.17
Transverse modulus for glass/epoxy according to Tsai–Hahn equation (equation [3.62]). (From Tsai, S.W. and Hahn, H.T. 1980. *Introduction to Composite Materials*. Technomic Publishing Co., Lancaster, PA. With permission from Technomic Publishing Co.)

experimental data for the transverse modulus of a glass/epoxy composite compared with the predicted values from equation (3.62) for two different assumed values of the stress-partitioning parameter. The stress-partitioning parameter $\eta_2 = 0.5$ was found to yield accurate predictions of G_{12} based on comparisons with experimental data for the same glass/epoxy [10]. Formulas for estimating the stress-partitioning parameters from constituent material properties are also given in [10].

3.6 Problems

1. A rectangular array of elliptical fibers is shown in figure 3.18. Derive the relationship between the fiber volume fraction and the given geometrical parameters. What is the maximum possible fiber volume fraction for this packing geometry?
2. The fibers in a E-glass/epoxy composite are 0.0005 in (0.0127 mm) in diameter before coating with an epoxy sizing 0.0001 in (0.00254 mm) thick. After the sizing has been applied, the fibers are bonded together with more epoxy of the same type. What is the maximum fiber volume fraction that can be achieved? Using the fiber and matrix moduli given in equation (3.29), determine the composite longitudinal modulus E_1 and the composite transverse modulus E_2 corresponding to the maximum fiber volume fraction.
3. A hybrid carbon-aramid/epoxy composite is made by randomly mixing continuous aligned fibers of the same diameter, so that there are two carbon fibers for each aramid fiber. The fibers are assumed to be arranged in a square array with the closest possible

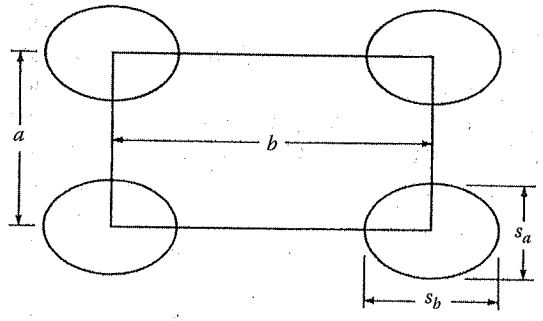

FIGURE 3.18
Rectangular array of elliptical fibers.

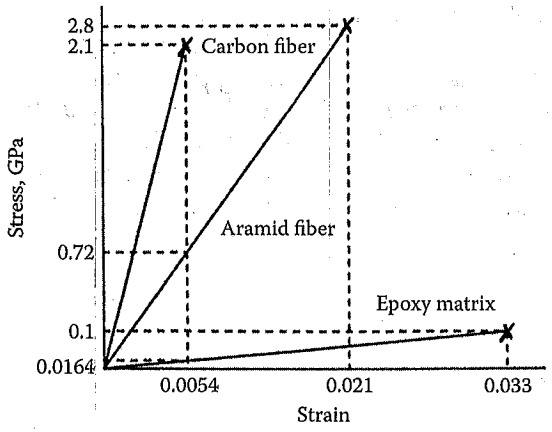

FIGURE 3.19
Stress–strain curves for fiber and matrix materials in a hybrid composite.

packing. The stress–strain curves for longitudinal tensile loading of fiber and matrix materials are shown in figure 3.19. Determine the composite longitudinal modulus E_1.

4. Derive equation (3.41).
5. Derive equation (3.43).
6. Using an elementary mechanics of materials approach, find the micromechanics equation for predicting the minor Poisson's ratio, ν_{21}, for a unidirectional fiber composite in terms of the corresponding fiber and matrix properties and volume fractions. Assume that the fibers are orthotropic, the matrix is isotropic, and all materials are linear elastic. This derivation should be independent of the one in problem 4.
7. A composite shaft is fabricated by bonding an isotropic solid shaft having shear modulus G_1, and outside radius r_1, inside a hollow isotropic shaft having shear modulus G_2 and outside radius r_2. The composite shaft is to be loaded by a twisting moment, T, that is distributed over the end of the shaft, as shown in figure 3.20. Using an elementary mechanics of materials approach, derive the equations for the stresses and deformations at any radius and the equation for the effective torsional shear modulus of the composite shaft in terms of the material and geometrical properties of shafts 1 and 2.
8. Using the method of subregions, derive an equation for the transverse modulus, E_2, for the RVE, which includes a fiber/matrix

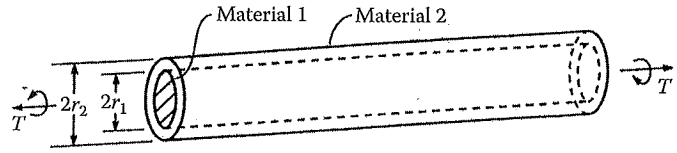

FIGURE 3.20
Composite shaft under torsional load.

interphase region, as shown in figure 3.21. *Hint*: The equation should reduce to equation (3.50) when the fiber diameter is the same as the interphase diameter.

9. Derive equation (3.55).
10. For a unidirectional composite with a rectangular fiber array (fig. [3.10]), use the equations of elasticity to set up the displacement boundary value problem for determination of the transverse modulus, E_2. That is, find the governing partial differential equations for displacements u and v in the RVE, and specify the boundary and continuity conditions. Assume plane strain ($\varepsilon_z = 0$). Do not attempt to solve the equations, but explain briefly how E_2 would be found. Assume that both fiber and matrix are isotropic.
11. Derive equation (3.62).
12. Show that a value of $\xi = 0$ reduces the Halpin–Tsai equation (eq. [3.59]) to the inverse rule of mixtures (eq. [3.36]), whereas a value $\xi = \infty$ reduces it to the rule of mixtures (eq. [3.23]).

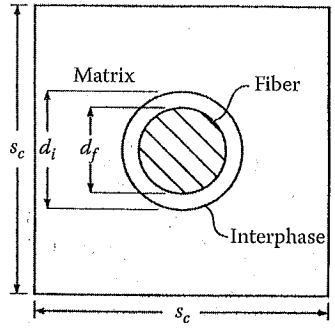

FIGURE 3.21
RVE with fiber/matrix interphase region.

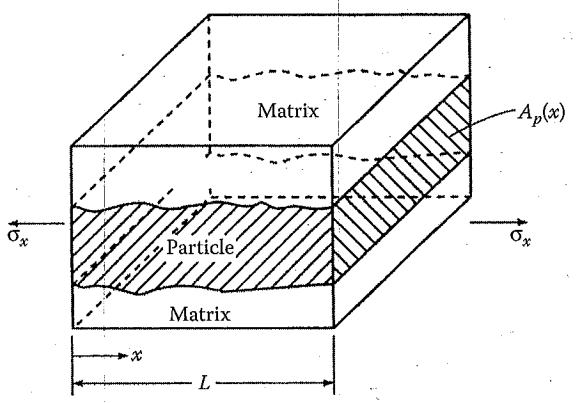

FIGURE 3.22
RVE for a particle-reinforced composite with a particle that has a varying cross-sectional area $A_p(x)$.

13. An RVE from a particle-reinforced composite is shown in figure 3.22. The particle has a cross-sectional area $A_p(x)$ that varies with the distance x, and the stresses and strains in particle and matrix materials also vary with x. Find the expression for the effective Young's modulus of the composite, E_x, along the x direction. The answer should be left in terms of an integral involving the length, L; the particle modulus, E_p; the matrix modulus, E_m; and the particle area fraction $a_p(x) = A_p(x)/A_c$, where A_c is the total composite cross-sectional area. Assume that both the particle and the matrix are isotropic.
14. Using the result from problem 13, determine the effective Young's modulus, E_x, for the RVE shown in figure 3.23. In figure 3.23 the

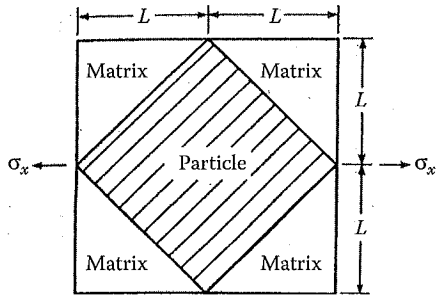

FIGURE 3.23
RVE for a composite reinforced with a square particle and loaded along the diagonal of the particle.

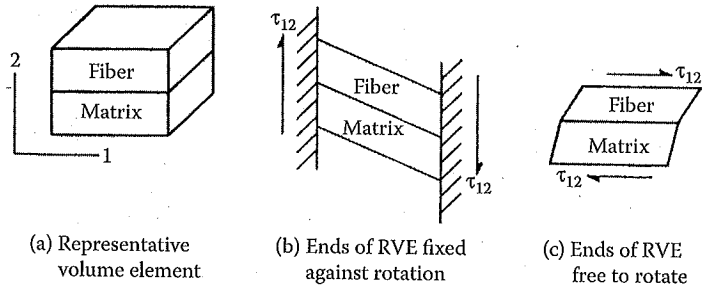

(a) Representative volume element (b) Ends of RVE fixed against rotation (c) Ends of RVE free to rotate

FIGURE 3.24
RVE with two different loading and boundary conditions for problem 15.

reinforcing particle has a square cross section and is oriented as shown. For a particle having a Young's modulus $E_p = 10 \times 10^6$ psi (68.95 GPa) and a matrix having a Young's modulus $E_m = 0.5 \times 10^6$ psi (3.45 GPa), determine the value of E_x and compare with the values from the rule of mixtures (eq. [3.23]) and the inverse rule of mixtures (eq. [3.36]). Discuss your results in the context of the comments on theoretical bounds on the transverse modulus in section 3.4.

15. A unidirectional composite is to be modeled by the RVE shown in figure 3.24(a), where the fiber and matrix materials are assumed to be isotropic and perfectly bonded together. Using a mechanics of materials approach, derive the micromechanics equations for the effective in-plane shear modulus, G_{12}, for the following cases:
    a. The ends of the RVE are perfectly bonded to supports that are rigid against rotation, then subjected to the uniform in-plane shear stress, τ_{12}, by the nonrotating supports, as shown in figure 3.24(b).
    b. The top and bottom surfaces of the RVE are subjected to the uniform in-plane shear stress, τ_{12}, and the ends of the RVE are free to rotate, as shown in figure 3.24(c).
16. Figure 3.25 shows an RVE for an elementary mechanics of materials model of the same type as shown in figure 3.5, but with transverse deformation along the 2 direction prevented by rigid supports along the top and bottom edges. For an applied longitudinal normal stress as shown in figure 3.25, find a micromechanics equation for the longitudinal modulus E_1. Do not neglect the Poisson strains in the general derivation, and show what happens to the general equation for E_1 when the Poisson's ratios for composite, fiber, and matrix are all equal.

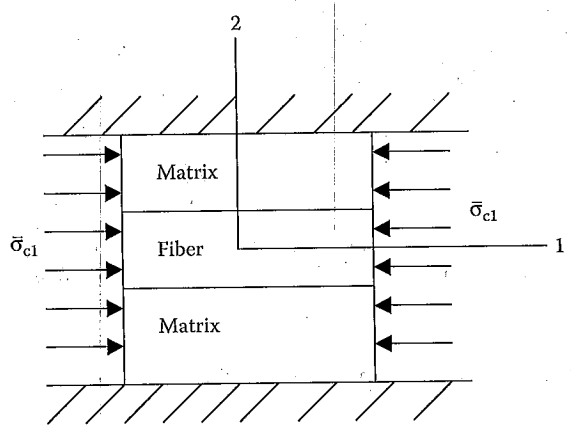

FIGURE 3.25
RVE for elementary mechanics of materials model with rigid supports that prevent transverse deformation.

References

1. Hashin, Z. 1983. Analysis of composite materials — A survey. *Journal of Applied Mechanics*, 50, 481–505.
2. Chamis, C.C. and Sendeckyj, G.P. 1968. Critique on theories predicting thermoelastic properties of fibrous composites. *Journal of Composite Materials*, 2(3), 332–358.
3. Christensen, R.M. 1979. *Mechanics of Composite Materials*. John Wiley & Sons, New York.
4. Halpin, J.C. 1984. *Primer on Composite Materials: Analysis* (rev.). Technomic Publishing Co., Lancaster, PA.
5. Gibson, R.F. 1975. Elastic and dissipative properties of fiber reinforced composite materials in flexural vibration. Ph.D. Dissertation, University of Minnesota.
6. Yang, H. and Colton, J.S. 1994. Microstructure-based processing parameters of thermoplastic composite materials. Part I: Theoretical models. *Polymer Composites*, 51(1), 34–41.
7. Adams, R.D. 1987. Damping properties analysis of composites, in Reinhart, T.J. et al. eds., *Engineered Materials Handbook*, vol. 1, *Composites*, pp. 206–217. ASM International, Materials Park, OH.
8. Whitney, J.M. and Riley, M.B. 1966. Elastic properties of fiber reinforced composite materials. *AIAA Journal*, 4(9), 1537–1542.
9. Gibson, R.F. and Plunkett, R. 1976. Dynamic mechanical behavior of fiber-reinforced composites: Measurement and analysis. *Journal of Composite Materials*, 10, 325–341.

10. Tsai, S.W. and Hahn, H.T. 1980. *Introduction to Composite Materials*. Technomic Publishing Co., Lancaster, PA.
11. Jones, R.M. 1999. *Mechanics of Composite Materials*, 2d ed. Taylor and Francis, Philadelphia, PA.
12. Hopkins, D.A. and Chamis, C.C. 1988. A unique set of micromechanics equations for high temperature metal matrix composites, in DiGiovanni, P.R. and Adsit, N.R. eds., *Testing Technology of Metal Matrix Composites*, ASTM STP 964, pp. 159–176. American Society for Testing and Materials, Philadelphia, PA.
13. Drzal, L.T., Rich, M.J., Koenig, M.F., and Lloyd, P.F. 1983. Adhesion of graphite fibers to epoxy matrices. II. The effect of fiber finish. *Journal of Adhesion*, 16, 133–152.
14. Chamis, C.C. 1984. Simplified composite micromechanics equations for hygral, thermal and mechanical properties. *SAMPE Quarterly*, 15(3), 14–23.
15. Chamis, C.C. 1987. Simplified composite micromechanics equations for mechanical, thermal and moisture-related properties, in Weeton, J.W., Peters, D.M., Thomas, K.L. eds., *Engineers' Guide to Composite Materials*. ASM International, Materials Park, OH.
16. Kriz, R.D. and Stinchcomb, W.W. 1979. Elastic moduli of transversely isotropic graphite fibers and their composites. *Experimental Mechanics*, 19, 41–49.
17. Kowalski, I.M. 1986. Determining the transverse modulus of carbon fibers. *SAMPE Journal*, 22(4), 38–42.
18. Kawabata, S. 1988. Measurements of anisotropic mechanical property and thermal conductivity of single fiber for several high performance fibers. *Proceedings of 4th Japan–U.S. Conference on Composite Materials*, pp. 253–262, Washington, D.C.
19. Caruso, J.J. and Chamis, C.C. 1986. Assessment of simplified composite micromechanics using three-dimensional finite element analysis. *Journal of Composites Technology and Research*, 8(3), 77–83.
20. Spencer, A. 1986. The transverse moduli of fibre composite material. *Composites Science and Technology*, 27, 93–109.
21. Adams, D.F. and Doner, D.R. 1967. Longitudinal shear loading of a unidirectional composite. *Journal of Composite Materials*, 1, 4–17.
22. Adams, D.F. and Doner, D.R. 1967. Transverse normal loading of a unidirectional composite. *Journal of Composite Materials*, 1, 152–164.
23. Caruso, J.J. 1984. Application of finite element substructuring to composite micromechanics. NASA TM 83729.
24. Finegan, I.C. and Gibson, R.F. 1997. Analytical and experimental characterization of damping and stiffness in polymer composites having coated fibers as reinforcement, in Farabee, T.M. (ed.), *Proceedings of ASME Noise Control and Acoustics Division*, NCA-Vol.24, pp. 127–138.
25. Finegan, I.C. and Gibson, R.F. 1998. Improvement of damping at the micromechanical level in polymer composite materials under transverse normal loading by the use of special fiber coatings. *Journal of Vibration and Acoustics*, 120(2), 623–627.
26. Whitney, J.M. 1967. Elastic moduli of unidirectional composites with anisotropic fibers. *Journal of Composite Materials*, 1, 188–193.

27. Aboudi, J. 1989. Micromechanical analysis of composites by the method of cells. *Applied Mechanics Reviews*, 42(7), 193–221.
28. Paul, B. 1960. Prediction of elastic constants of multi-phase materials. *Transactions of AIME*, 218, 36–41.
29. Hashin, Z. and Rosen, B.W. 1964. The elastic moduli of fiber reinforced materials. *Journal of Applied Mechanics*, 31, 223–232. Errata, p. 219 (March 1965).
30. Torquato, S. 1991. Random heterogeneous media: microstructure and improved bounds on effective properties. *Applied Mechanics Reviews*, 44(2), 37–76.
31. Halpin, J.C. and Tsai, S.W. 1969. Effects of environmental factors on composite materials. AFML-TR-67–423.

4

Strength of a Continuous Fiber-Reinforced Lamina

4.1 Introduction

Because of the variety of failure modes that can occur in composites, the analysis of composite strength is more difficult than the analysis of elastic behavior, which was discussed in chapter 2 and chapter 3. As shown in chapter 1, the strength of a composite is derived from the strength of the fibers, but this strength is highly directional in nature. For example, the longitudinal strength of the continuous fiber-reinforced lamina, s_L, is much greater than the transverse strength, s_T. In addition, the compressive strengths $s_L^{(-)}$ and $s_T^{(-)}$ associated with these directions may be different from the corresponding tensile strengths $s_L^{(+)}$ and, $s_T^{(+)}$, and the transverse tensile strength $s_T^{(+)}$ is typically the smallest of all the lamina strengths for reasons that will be explained later. The in-plane shear strength s_{LT} associated with the principal material axes is still another independent property. These five lamina strengths form the basis of a simplified lamina strength analysis, which will, in turn, be used later in a simplified laminate strength analysis. The relationships among these five lamina strengths and the allowable lamina strengths under off-axis or multiaxial loading are discussed in this chapter, as are several micromechanical models for predicting the lamina strengths. Interlaminar strengths will be discussed in chapter 7 and chapter 9.

As shown in chapters 2 and chapter 3, the linear elastic stress–strain relationships for the orthotropic lamina are simplified by the use of "effective moduli." The effective moduli, which relate the volume-averaged lamina stresses to the volume-averaged lamina strains [recall equation (2.7) to equation (2.9)], are defined by simple uniaxial or shear stress conditions associated with the lamina principal material axes. Using a similar approach, the "effective strengths" of the lamina may be defined as ultimate values of the volume-averaged stresses that cause failure of the lamina under these same simple states of stress. The stress–strain curves in figure 4.1 show the graphical interpretation of these simple states of stress, the effective strengths $s_L^{(+)}$, $s_L^{(-)}$, $s_T^{(+)}$, $s_T^{(-)}$, and s_{LT}, and the corresponding